ELSEVIER

International Journal of Mass Spectrometry 177 (1998) 175–186

International Journal of Mass Spectrometry

Simplified injector flanges for the selected ion flow tube

Vyacheslav N. Fishman, Joseph J. Grabowski*

Department of Chemistry, University of Pittsburgh, Pittsburgh, PA 15260, USA

Received 2 January 1998; revised 5 May 1998; accepted 6 May 1998

Abstract

Dual hole-pattern injector flanges (Venturi inlets) for a selected ion flow tube have been fabricated and tested in order to identify an optimum balance of efficient operational characteristics and simplicity of fabrication, along with reproducible assembly. The diagnostic measurements for each configuration addressed: (a) ability to maintain pressure differences between ion selection and ion reaction regions; (b) ability to inject sufficient ions to carry out ion/molecule reaction studies; and (c) ability to not introduce turbulence in the reaction region of the flow tube. In addition, the sensitivity of these issues to different total gas flow and to partitioning of total flow between inner and outer injectors is considered. All hole-pattern injector configurations ever tried worked without requiring any adjusting. Importantly, extensive kinetic measurements of one ion/molecule reaction for many configurations, gas loads, and partitions, indicate turbulence in the reaction region is never a problem for these injectors. An injector flange with a small total helium inlet area via 12 holes, in a planar surface, with the ion orifice slightly downstream of the helium inlet plane, has provided the best experimental data. (Int J Mass Spectrom 177 (1998) 175–186) © 1998 Elsevier Science B.V.

Keywords: Selected ion flow tube; SIFT; Flowing afterglow; Injector flange; Venturi inlet

1. Introduction

The SIFT (selected ion flow tube), developed by Adams and Smith [1,2], is a powerful instrument for studying ions, molecules, and their reactions, under well-defined thermal energy conditions, in the gas-phase. A SIFT is composed of an ion selection region, followed by a reaction region, and finally, a mass analyzer region (Fig. 1). As the SIFT's reaction region is a high pressure (e.g. 0.5 Torr) flow tube, the apparatus requires a specialized piece of hardware that both maintains a pressure gradient (between ion selection and reaction regions) and facilitates ion injection into the reaction region at sufficient ion intensity to allow one to carry out the reaction of interest [1–13]. These injector flanges (also called Venturi inlets) are designed to direct a high flow of buffer gas down the reaction tube in such a fashion that minimal gas load backflows into the ion selection region, while simultaneously allowing fragile ions to be injected intact into the fast flow, high pressure reaction region. A third important characteristic of these inlets is to minimize turbulence in the well-characterized flow regime of the reaction tube. Injector flanges are believed to be the single most critical component on SIFT instruments. Two primary designs of SIFT injector flanges have been reported: the original "hole pattern" design by Adams and Smith [1], and a subsequent annulus design by Howorka et

* Corresponding author.

1387-3806/98/$19.00 © 1998 Elsevier Science B.V. All rights reserved
PII S1387-3806(98)14040-X

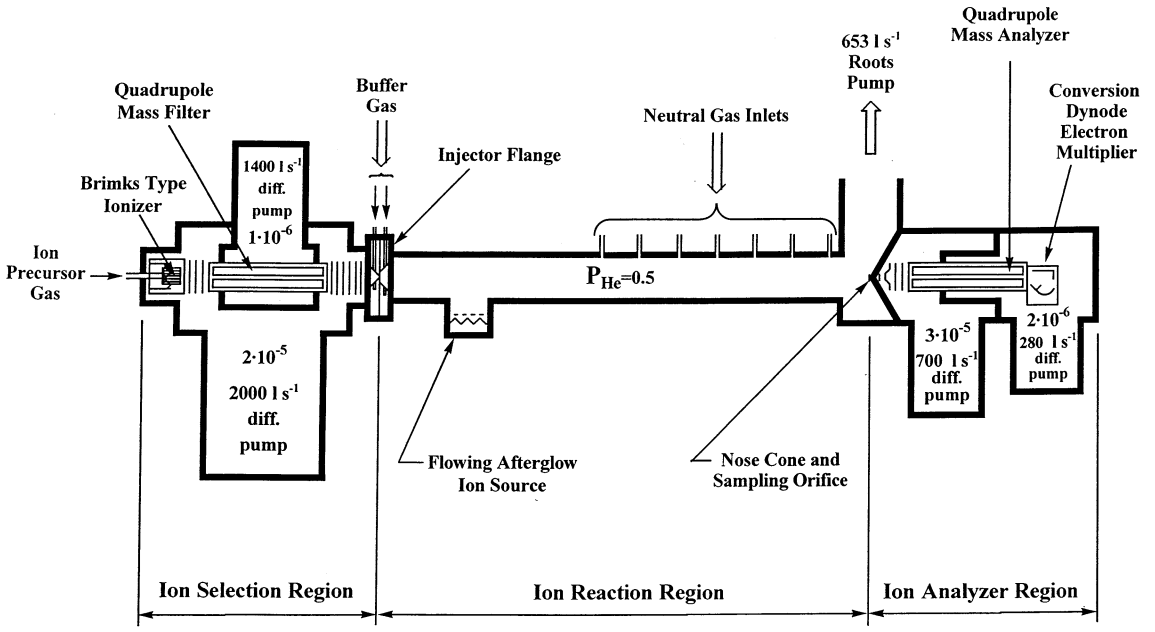

Fig. 1. A schematic diagram of the University of Pittsburgh's SIFT apparatus illustrating its major sections: the ion source/selection region, the ion reaction region, and the ion analysis/detection region. The pressures indicated are uncalibrated ion gauge tube readings for a typical experiment at a flow tube pressure of 0.5 Torr of helium (capacitance manometer measurement). The pumping speeds listed are for diffusion pumps and reflected values for air.

al. [3] and Mackay et al. [4]. Dupeyrat and co-workers [5], in 1982, evaluated the effectiveness of three different injector flanges, the so-called, Birmingham, NOAA I and NOAA II designs (e.g. Table 1). This study found that the cross-sectional area for buffer gas introduction inversely scaled with injector performance: As the total area decreased, the performance increased. However, as noticed by several groups, [4,6] smaller inlet areas increased turbulence in the critical portion of the flow tube as exemplified by anomalies in rate coefficient measurements. Specifically, it was observed that the apparent value of a rate coefficient decreased significantly as a greater fraction of the total buffer gas flow was introduced to the flow tube through the inlet with smaller area. One solution to the turbulence problem identified was to incorporate a "damping region" of sufficient length between the injector and measurement region [5]. An alternative solution was achieved by Mackay et al. [4] via the incorporation of a second buffer gas inlet and a partitioning of the gas load between two rather different inlets. In this fashion, a combination of supersonic and subsonic flows minimized the turbulence problem. Recognizing the versatility of the two inlet injector flange, Van Doren and co-workers [7,8] have designed a dual injector that has become the defacto standard and has been adopted by several research groups [10,11].

The dual annulus design [7,8] for injector flanges has achieved a reputation of requiring high tolerances in machining, difficulty in assembly, and ambiguity in assessing all spatial parameters [10]. A dual injector flange with both inlets based on a series of holes (i.e. following the lead of the original Birmingham design) offers the potential of solving several of these problems, but has not been tested previously. Furthermore, the reduced expense of machining hole-pattern injectors provides an opportunity for varying a number of spatial parameters and evaluating their impact on performance. In this article, we report on the design, fabrication, and evaluation of a dual SIFT injector in which both inner and outer injectors are of the

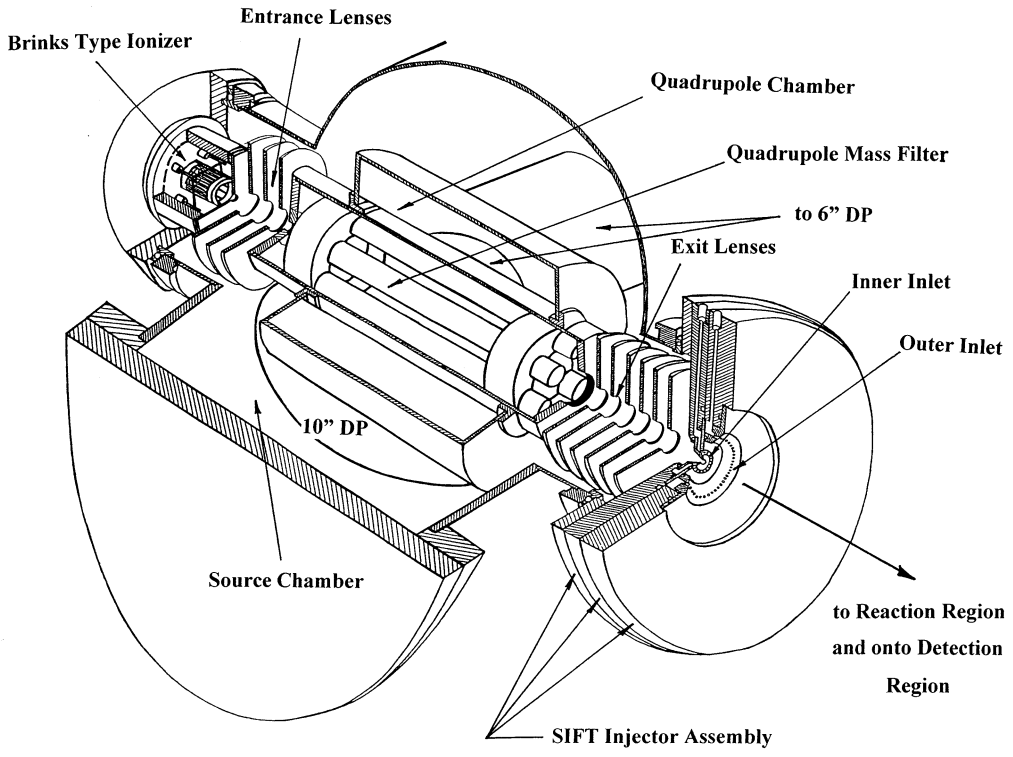

Fig. 2. Cut-away schematic diagram of the ion source/selection region of the SIFT.

"hole-pattern" type. In what follows, we use *injector* to refer to the entire assembly and *inlet* to refer to individual inner or outer components. Thus, our injector is composed of an inner and outer inlet.

2. Apparatus

The SIFT at the University of Pittsburgh (Fig. 1) is composed of source, reaction, and analysis regions. In the source region, ions are created in a Brinks type source [14] (high pressure and flow tube sources are also available but have not been used in this work), then ions of one charge type are extracted from the ion source and focused through three lens elements into a quadrupole mass filter (the path from ion source to quadrupole case is 3.3 cm). The quadrupole is housed in a separately pumped region to enhance its operating characteristics. The mass-to-charge-selected ions exit the quadrupole and are refocused by six lens elements onto the orifice of the injector flange (the distance between quadrupole case and injector flange is 8.2 cm). The separation of quadrupole and injector flange is designed to maximize pumping efficiency behind the injector flange and to minimize pressure inside the quadrupole, both in order to achieve efficient separation and to minimize scattering losses.

Several other design criteria deserve mention. The three lens elements closest to the injector flange are fabricated, in part, from perforated steel in an attempt to increase pumping efficiency to the backside of the injector flange. The injector flange is electrically insulated from the ion selection and ion reaction regions and is usually biased for optimum focusing of ions into the flow tube. In order to improve transmission, the leaky-dielectric elements at both ends of the quadrupole were removed [7,8]. The ion source/selection region, shown in a cut-away view in Fig. 2, is pumped by an Edwards Diffstak 250 M diffusion pump (2000 l s^{-1}, air). The quadrupole mass filter

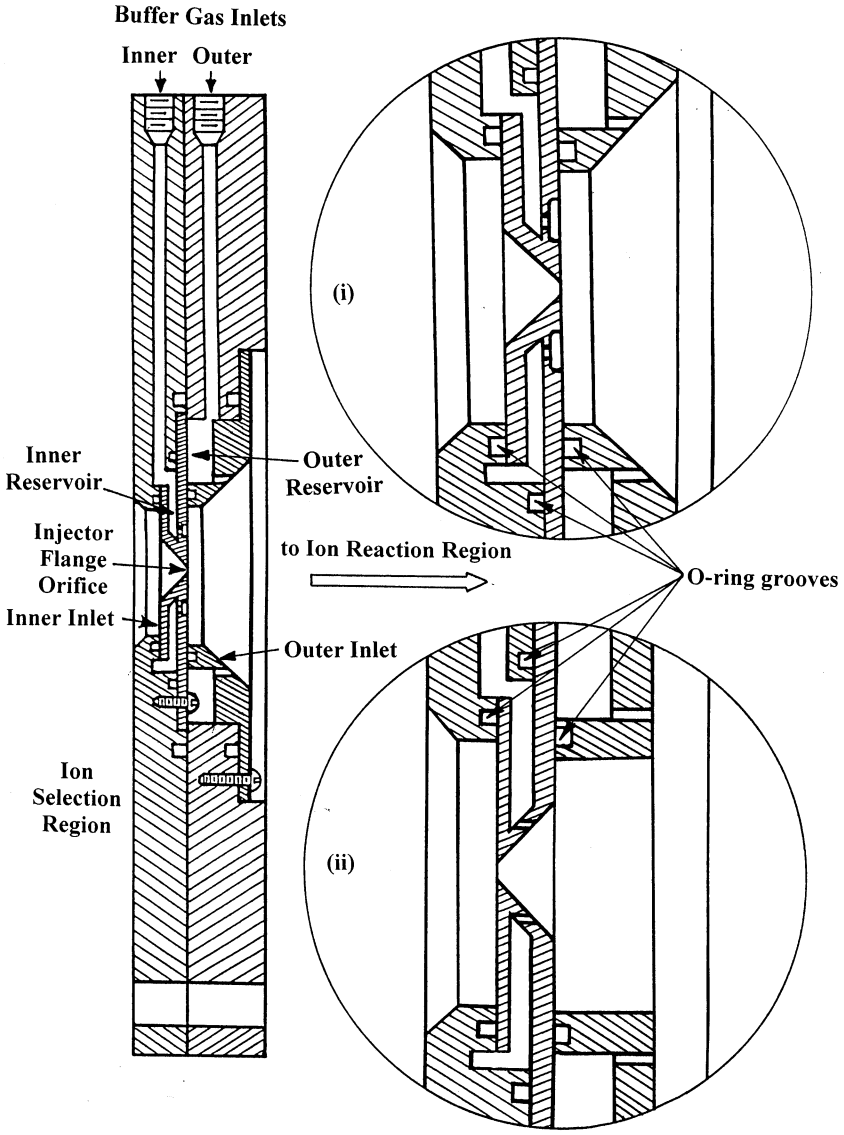

Fig. 3. Overview of assembled injector flange and enlarged views of: (i) inner inlet-D/outer inlet-B; and (ii) inner inlet-B/outer inlet-A.

(ABB Extrel Model 7-324-9; 19 mm diameter × 22 cm rods; 1–340 u mass range) is separately pumped by a Varian VHS-6 diffusion pump equipped with an optional Mexican Hat Cold Cap and high conductance gate valve (1400 l s^{-1}, air). Both diffusion pumps were initially backed by a common Leybold-Heraeus D30A Mechanical pump (12.6 l s^{-1}, air), but most recently were reconfigured to be independently pumped: the 250 M by the D30A and the VHS-6 by a Pfeiffer Balzers UNO-016B (4.4 l s^{-1}, air) mechanical pump. Use of two mechanical pumps gives a slight improvement (versus one mechanical pump) of ~10% decrease in pressure in both sections of the ion source region, for 0.4–0.5 Torr of helium in the reaction region.

The selected ion beam is injected into the reaction region at the lowest possible energy, through the 2-mm-diameter orifice in the injector flange. The

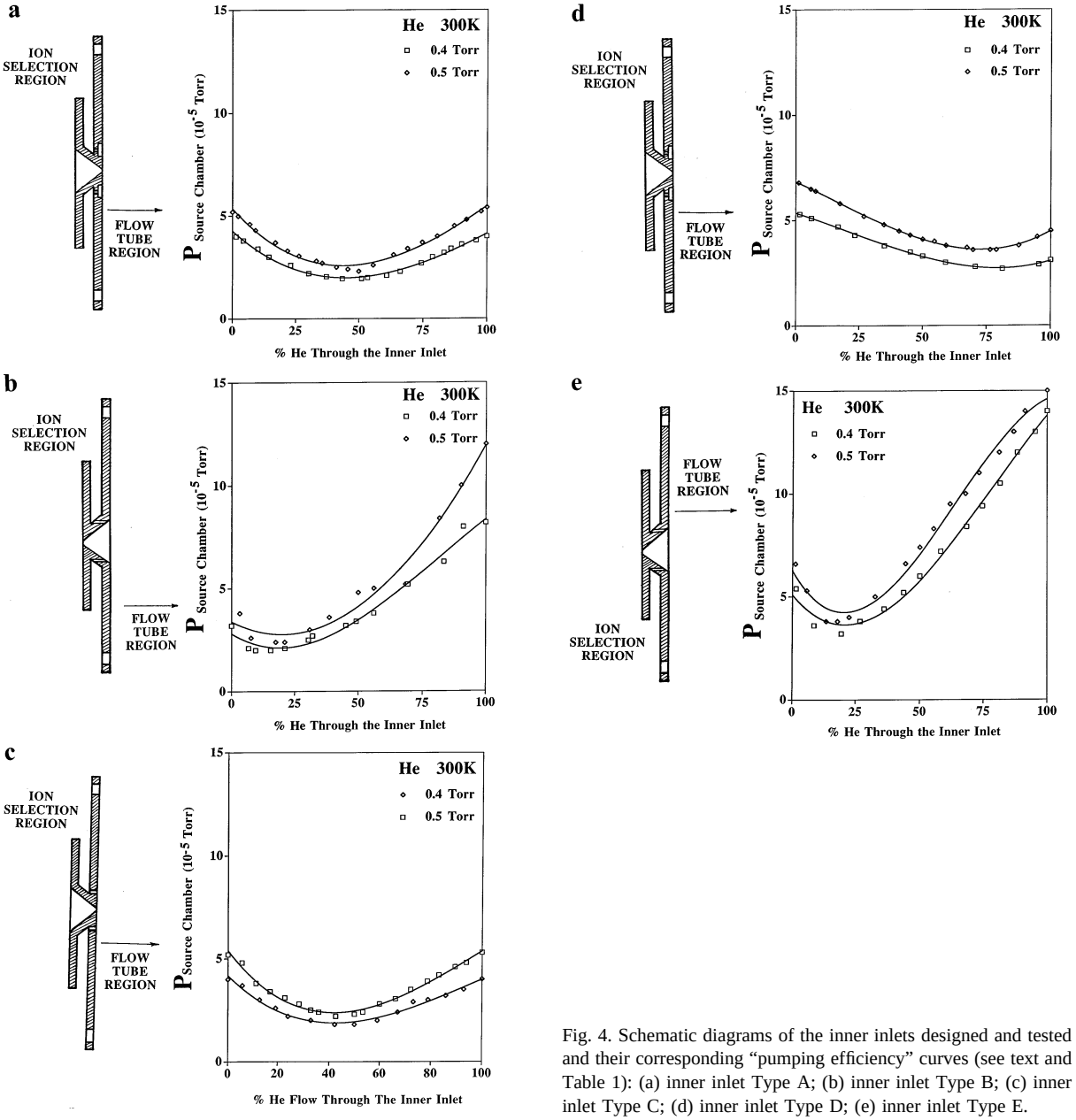

Fig. 4. Schematic diagrams of the inner inlets designed and tested and their corresponding "pumping efficiency" curves (see text and Table 1): (a) inner inlet Type A; (b) inner inlet Type B; (c) inner inlet Type C; (d) inner inlet Type D; (e) inner inlet Type E.

reaction region is a stainless steel flow tube (150 cm long by 7.3 cm i.d.), connected at the upstream to the injector flange and at the downstream end to the pumping (exhaust) line for the mechanical pump booster system. The flow tube pressure can be maintained at any desired pressure between 0.2–2 Torr. For the work reported here, a helium flow of 145–200 STP $cm^3\ s^{-1}$, corresponding to a flow tube pressure of 0.4–0.5 Torr, is maintained by a Leybold-Heraeus pumping station (WA2000/S250; 653 $l\ s^{-1}$, air), and is characterized by a velocity of ~7000–8000 cm s^{-1}. The helium serves two main purposes: to transport the ions and neutral reactants from their introduction points, down the flow tube, to the analysis

region, and also to ensure that the reacting species are thermally equilibrated to the temperature of the flow tube (for us, room temperature, 298–300 K). For purity reasons, the helium (4.7 grade/99.997%) is passed through a 292 cm long by 1.6 cm i.d. trap filled with a uniform mixture of 3A, 4A, and 13X molecular sieves and immersed in liquid nitrogen during use (the trap is routinely reactivated by baking/pumping overnight).

The reaction region also contains a number of neutral addition ports, including 10 uniformly spaced radial inlets [15,16]. A constant flow of neutral reactant is typically introduced into the system at one of seven different distances (corresponding to Ports 1–7) with the largest being 76.7 and the smallest 16.1 cm from the sampling orifice; each distance corresponds to a different reaction time.

At the end of the flow tube, a fraction of the ions are sampled through a 1-mm-diameter hole in a 0.25 mm thick by 2-cm-diameter molybdenum orifice plate. This orifice plate demarcates the boundary between the reaction region and the second mass filter maintained in the analyzer region. An ion extractor [2] containing a 2 mm aperture is located 0.8 mm behind the orifice to increase ion sampling efficiency. The "nose cone" holding this orifice/extractor assembly is itself electrically insulated from the assembly and from ground (routinely, however, we find that grounding or biasing the "nose cone" has no impact on detected ion signals). A set of three electrostatic lenses behind the extractor is physically mounted to the ELFS mounting plate on the front of the quadrupole and serves to focus ions into the quadrupole mass analyzer. Ions that successfully transit the mass filter interact with a conversion dynode electron multiplier with a gain of $\sim 10^8$. A variety of instrumental parameters can be brought under computer control using a custom-designed FORTH program to facilitate data collection.

The detection region is differentially pumped in a manner similar to that for source region. The detection region immediately behind the sampling orifice is pumped by an Edwards Diffstak 160 M diffusion pump (700 l s^{-1}, air) while the quadrupole mass filter (ABB Extrel Model 7-270-9; 16 mm diameter × 22 cm rods; 1–500 u mass range and Detector Technology, Inc. Model 402S conversion dynode electron multiplier) is pumped by an Edwards Diffstak 100 M diffusion pump (280 l s^{-1}, air). Both of these diffusion pumps are backed by a common Edwards E2M18 Rotary vacuum pump (4.7 l s^{-1}, air). Typical chamber pressures recorded during an experiment conducted at a flow tube pressure of 0.5 Torr (helium) are noted in Fig. 1 (uncalibrated ion gauge tube readings).

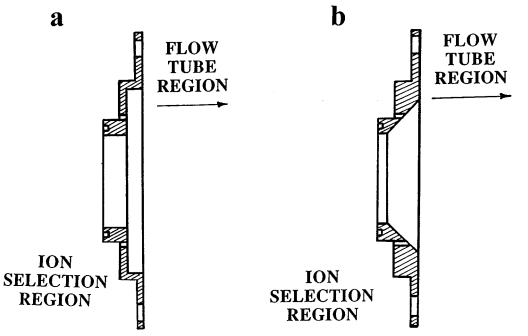

Fig. 5. Schematic diagrams of the outer inlets: (a) Outer inlet Type A; (b) Outer inlet Type B.

3. Results and discussion

We have designed and built a SIFT injector composed of easily modified and assembled inner and outer inlets, an overview of which is summarized in (Fig. 3). Each inlet is assembled from two pieces with the smaller, centerpiece bearing all the critical design parameters and the larger, outer piece providing the mechanical support and gas supply channel. Five different inner inlets (A, B, C, D, and E, Fig. 4) have been evaluated, along with two different outer inlets (A and B, Fig. 5). Each of the inlets we have constructed (both inner and outer) is composed of a single circular array of holes, symmetrically located around the 2 mm ion entrance orifice. Included in all designs is a high conductance helium reservoir "behind" the arrays to ensure uniform gas delivery through each hole in the array (Fig. 3). Several of the key design parameters for both the inlets evaluated

Table 1
SIFT injector flange inlet specifications.

Design	Type	Gas introduction area (mm^2)	Nominal diameter of gas inlet (mm)	Ion orifice diameter (mm)	Orifice-gas inlet separation (mm)	References
Birmingham (inner)	Holes: 12 × 1 mm	9.4	20	1 or 3	10	[2,5]
NOAA I (inner)	Annulus: width 0.41 mm	10.7	8.7	3	2.5	[5]
NOAA II (inner)	Annulus: width 0.025 mm	0.7	8.7	3	2.5	[5]
Boulder (inner)	Annulus: width 0.025 mm	0.7	8.7	2	3.5	[7,8]
Boulder (outer)	Annulus: width 0.81 mm	55.8	43.8	NA	20.9	[7,8]
Pitt-A (inner)	Holes: 12 × 0.34 mm	1.1	8.7	2	−0.9	This work
Pitt-B (inner)	Holes: 12 × 0.34 mm	1.1	7.9	2	4	This work
Pitt-C (inner)	Holes: 12 × 0.34 mm	1.1	8.7	2	0	This work
Pitt-D (inner)	Holes: 12 × 0.20 mm	0.4	11.1	2	−1.3	This work
Pitt-E (inner)	Holes: 24 × 0.20 mm	0.8	7.9	2	4	This work
Pitt-A (outer)	Holes: 36 × 1.4 mm	55.4	44.5	NA	14.4[a]	This work
Pitt-B (outer)	Holes: 36 × 1.4 mm	55.4	44.5	NA	8[b]	This work

NA: not applicable.
[a]See Fig. 3 (ii) for inner B and outer A.
[b]See Fig. 3 (i) for inner A and outer B.

here and others reported in literature are summarized in Table 1.

3.1. Effect of partitioning on gas load to ion selection region

One goal of the use of Venturi inlets is to reduce the backstreaming of gas from the high pressure reaction region into the low pressure ion selection region. We have evaluated how the inner injector (which outer injector is used is immaterial as both outer injectors performed identically in these tests) affects the pressure in the selection region for both 0.4 and 0.5 Torr of helium in the flow tube, and as the helium introduction is partitioned between the inner and outer injectors. We sought to understand how the inlet geometry, the total cross-sectional area of the inlet through which the gas is introduced, and the reaction region pressure, impact backstreaming. For all inner inlets, the total cross-sectional area for gas introduction is a conductance-limited element involving supersonic flow of a free jet expansion under continuum conditions [17]. It is believed that our circularly symmetric hole pattern (with respect to the ion introduction orifice), upon buffer gas addition, results in a considerably lower buffer gas density in a "cone" near the orifice with respect to any other pressure region inside the free jet or flow tube. These conditions give rise to the "Venturi effect" in which the gas pressure near the orifice in the flow tube is substantially reduced from the bulk pressure. The data for five different inner–outer injector flange configurations are shown in Fig. 4 while similar data for a dual-annulus injector has been described elsewhere [7,8].

Initial perusal of the five graphs in Fig. 4 demonstrates a wide variability in performance with inlet shape. For example, inlets A, B, and C have the same cross-sectional gas introduction area (Table 1) but different geometries; as a result, the minimum in the pressure curve (i.e. where we would prefer to operate) shifts from about 20% through the inner for inlet B to about 50% for inlets A and C. Inlet A has its buffer gas inlet plane slightly upstream of the orifice (−0.9 mm); however this offset has essentially no impact on the shape of its curve (similar curves for A and C; see Fig. 4). Thus, having an orifice "downstream," versus having an orifice in the same plane, of the helium inlet appears not to effect the partitioning of the gas load into the ion selection and reaction regions. Comparing B and E, two inlets with similar geometries but different total cross-sectional areas for their gas inlets, shows that both designs have their minimum in about

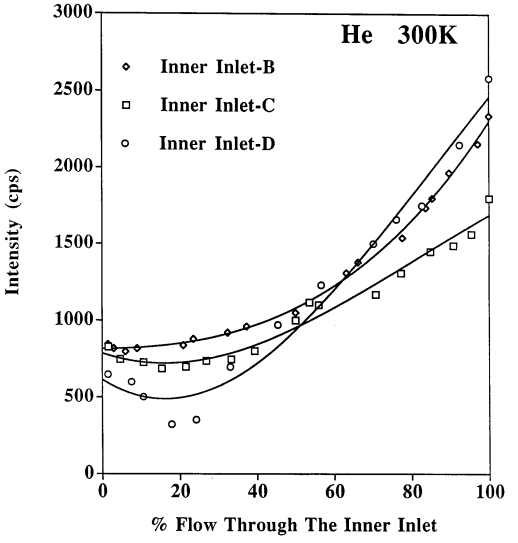

Fig. 6. Plot of detected $O^{\cdot+}$ ion intensity (cps) as a function of % buffer gas flow through the inner and outer inlets. For all three curves, the total pressure in the flow tube was held constant at 0.4 Torr of helium: Open diamond: inner-B/outer-B; open square: inner-C/outer-B; open circle: inner-D/outer-B. The data points are fit to arbitrary smooth curves to simplify comparisons.

the same place (i.e. ~20% through the inner inlet). We are not certain which of two reasons explains the dramatic change in curve shape for B and E (with respect to A, C, and D): either having the buffer gas inlet holes on the slope of the inner injector or having the ion entrance orifice behind (4 mm) the gas inlet plane; however, we expect that the differences are more likely due to the slope than the relative location. Comparing all curves in Fig. 4 shows that the minimum in the pressure for inlet-D is the closest of any to 100% through the inner (the point at which we find maximum signal, Fig. 6, vide infra). Only one apparently significant difference exists between inlets A, C, and D: D has the smallest gas inlet cross-sectional area. Finally, we note that machining of inner inlets A, C, and D is substantially easier than inner inlets B or E.

3.2. Inner/outer partitioning and injected signal

A dual inlet injector flange allows one to investigate the "efficiency" of ion injection as the buffer gas is added to the flow tube either through the smaller area of the inner injector or the larger area of the outer injector. For this test, we have chosen to use signal levels at the detection end (pulse counting system) as a measure of efficiency and to examine how that signal varied for an atomic ion as we changed the partition ratio; the data are summarized in Fig. 6. These data demonstrate that higher efficiency (i.e. more usable ions are transferred from the ion source region to the flow tube) is obtained as the fraction of the buffer gas added through the inner injector increases. For all cases examined (i.e. for all inner injectors, for all flow tube pressures, and for each ion investigated; not all data are shown) the maximum injected signal is always found when 100% of the gas is added via the inner injector. The data in Fig. 6 suggest that an increase in signal of 2.5–3 times is attainable by changing the helium partition from 100% through the outer to 100% through the inner inlet. These data, however, do not address backstreaming of gas into the source region (vide supra) or turbulence issues in the flow tube (vide infra). We should also point out that due to normal signal intensity fluctuations from week to week, it is not the absolute signal level in Fig. 6 that is of importance, but rather the shape of the curve. The shapes of the curves in Fig. 6 are essentially independent of ion source operating characteristics.

3.3. Evaluation of the Venturi effect

Dupeyrat et al. [5] previously have demonstrated one method for evaluating an injector flange's "Venturi inlet" capability—by directly measuring its ability to maintain a pressure gradient. This evaluation is conducted by isolating the selection region from all pumps except the "pumping action" of the Venturi injector. The data for measuring the pressure gradient across our injectors are displayed in Fig. 7, for the case when the total gas flow (helium) is directed through the inner inlet. Fig. 7 indicates that neither of our inlets is a good "pump" and that inlet D is able to maintain the largest pressure gradient ($P_{RR}/P_{SC} \sim 1.2$) in the operating region of interest ($120 < F_{He} < 160$ STD $cm^3\ s^{-1}$). Note that the curve for inner inlet Type-A has a similar shape to that for inlet Type-D; both of these injectors have the ion-entrance

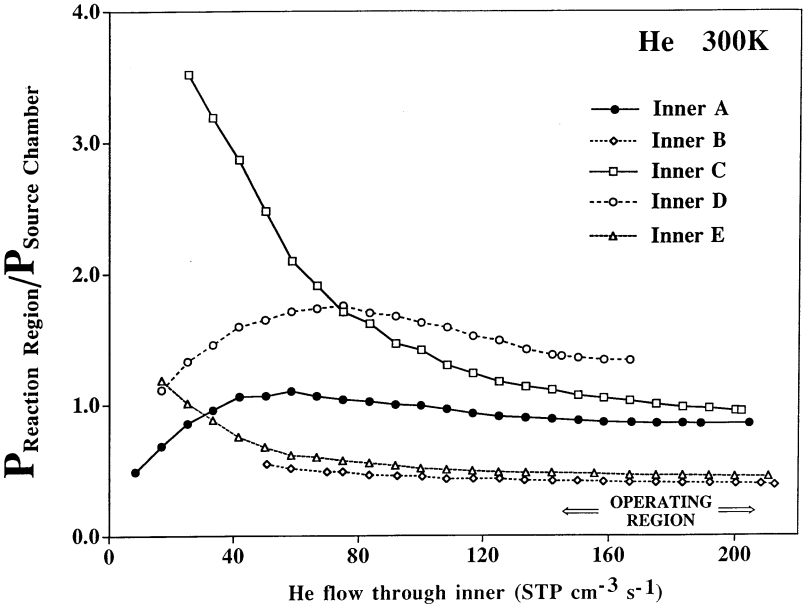

Fig. 7. Plot of pressure in the reaction region to that in the source chamber of the selection region (all selection region pumps are off) versus 100% helium flow through the indicated inner inlet.

orifice slightly downstream of the helium inlet plane [Fig. 4(a) and Fig. 4(d)]. Comparing the curves for inlets B and E [(Fig. 4(b) and Fig. 4(e)] in Fig. 7 shows that both designs with similar geometries have similar "pumping" behavior in the operational region ($P_{RR}/P_{SC} \sim 0.5$). Inner inlet Type-C [Fig. 4(c)] has the ion entrance orifice and helium inlet in the same plane; in Fig. 7 the graph for inlet C is quite different from these described above but is similar to inlets A and D in the operating region. It is important to note that for this series of experiments, we did not evaluate each injector at the partitioning fraction indicated by the minimum for that injector (Fig. 4). Comparison of the data in Fig. 7 with a similar figure by Dupeyrat et al. [5] shows that the NOAA II annulus injector is a more effective "pump" even though the gas inlet cross-sectional area for NOAA II is larger than our inner Type-D. However, "pumping effectiveness" (e.g. ability to minimize backstreaming) is but one criteria for inlet design/optimization.

3.4. Turbulence

The ideal SIFT injector should introduce no turbulence into the reaction region (i.e. should allow a

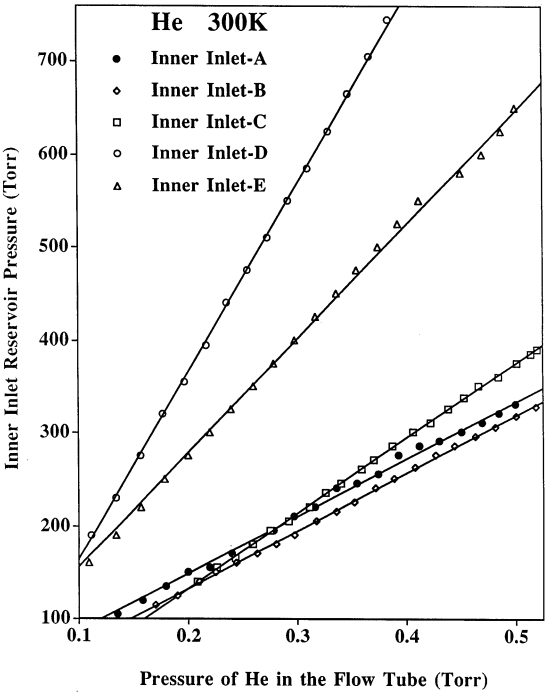

Fig. 8. Graphical representation of how the reservoir pressure behind the inner inlet varies as the flow tube pressure changes, for the case when all gas is added through the inner inlet. For each inlet, the data have been fit to a straight line.

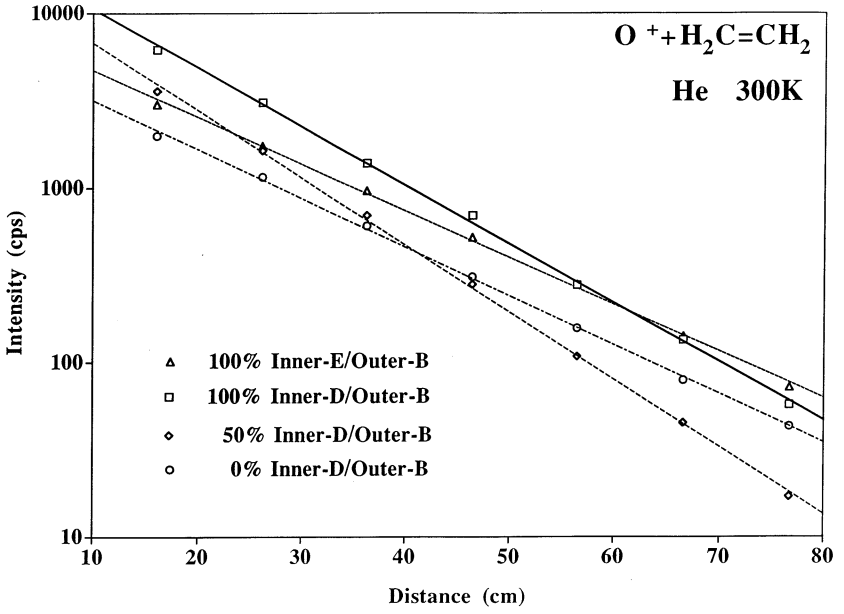

Fig. 9. Representative experimental SIFT data for determination of the bimolecular rate coefficient for the reaction of $O^{\cdot+}$ with $H_2C{=}CH_2$ as measured under pseudo-first-order kinetic conditions ($P_{He}/F_{ethylene}$) (Torr/STP $cm^3\ s^{-1}$): open triangle: 0.45/0.00620; open square: 0.49/00860; open diamond: 0.5/0.01048; open circle: 0.45/0.00710). Intensity data is an average cps determined for a total counting time per point of 5 s.

laminar profile to be achieved as rapidly as in a flowing afterglow) [2]. Flow structure for a pinhole expansion has been studied by Bier and Schmidt [18] and discussed by Miller [17]. The velocity of buffer gas (He) rises quickly immediately after the inlet while the magnitude of this velocity depends on the stagnation pressure and temperature of the inlet reservoir as well as the background pressure (in our case, pressure in the flow tube) [17]. Figure 8 is a plot of reservoir pressure versus flow tube pressure when all buffer gas is added through the indicated inner inlets. Inlet D, our inlet most likely to have turbulence problems, (i.e. the inlet with the smallest gas inlet area) requires a reservoir pressure of 850 Torr to achieve a flow tube pressure of 0.45 Torr. To reach 0.45 Torr in the reaction region, inner inlets A, B, and C require ~300 Torr and E requires a pressure of ~500 Torr in their reservoirs. Both outer inlets, A and B, require a pressure of ~115 Torr of helium in their reservoirs to reach 0.45 Torr in the reaction region (100% through the outer).

Experimentally, turbulence in a flow tube is often revealed by anomalies in kinetic measurements [4,6]. Therefore, we have made a number of measurements of the bimolecular rate coefficient for $O^{\cdot+}$ with ethylene under widely varying inlet usage conditions; a portion of this data is presented in Fig. 9 in the form of pseudo-first-order kinetics plots. For this test we used inner inlet D, as this inlet is the most likely one to have a turbulence problem. Inspection of Fig. 9 reveals the desired linear behavior for all operating conditions. Even for addition of the entire gas flow through the inner inlet, straight-line kinetic plots are obtained. Linear graphs are not necessarily sufficient to deduce the absence of turbulence; however the rate coefficients derived from the data shown in Fig. 9 are. The kinetics data for $O^{\cdot+}$ + $H_2C{=}CH_2$ obtained under a variety of conditions (including those displayed in Fig. 9) are summarized in Table 2. The data demonstrate that there are no systematic trends of derived rate coefficient with conditions that one would expect to indicate the presence of turbulence. We interpret the rate coefficient obtained, 1.40 ($\pm$0.07) $\times$ 10^{-9} $cm^3\ s^{-1}$, and the small error (4.7%,

Table 2
Rate coefficients for the reaction of $O^{\cdot+} + H_2C{=}CH_2$.

Inner inlet	% through inner[a]	No. of experiments	k_{obs} (cm^3 $molecule^{-1}$ s^{-1})
Inner-D	100	2	1.37×10^{-9}
Inner-D	50	2	1.31×10^{-9}
Inner-D	0	2	1.34×10^{-9}
Inner-E	100	8	1.44×10^{-9}
All	0–100	14	1.40×10^{-9}

[a]Outer Type B was used for all experimental data.

one σ, $n = 14$) as proof of the absence of turbulence in the reaction region of our SIFT. Undoubtedly, the 70 cm of flow tube between the injector flange and the start of the 80 cm long kinetic measurement region aid us in this regard.

3.5. Operating characteristics

In this final section we provide selected operational characteristics of our SIFT equipped with the injectors described above. Typical (uncalibrated) ion gauge tube reading for the various chambers are shown in Fig. 1 for an experiment conducted at 0.5 Torr of He (reaction region). Ion densities in the ion reaction region have been estimated for $O^{\cdot+}$ generated from electron ionization of CO_2. The ion density 27 cm downstream of the injector flange, at 0.45 Torr of He, is estimated as $\sim 2.4 \times 10^4$ cm^{-3} based upon current measurements on a movable probe (3 cm $\times$ 0.16 cm diameter) biased at -0.05 V and inserted perpendicular to the flow direction. That ion density falls to about 50 cm^{-3} at the orifice plate (123 cm further downstream), based on current measurements on the 2-cm-diameter orifice plate. This change in density is in accord with expected density changes due to "free" diffusion losses ($K_0[O^{\cdot+}] = 22.0 \pm 1.8$ cm^2 V^{-1} s^{-1}) [19].

4. Conclusions

We found that all "hole-pattern" type inner inlets so far tested work and none demonstrate any turbulence problem. The hole-pattern inlets are relatively easy to machine—ours are constructed of aluminum and are fabricated using drill bits (laser-drilled holes are an option we considered but found no advantage to pursue). Perhaps most importantly, the hole-pattern inlets require no critical alignment during installation—we simply bolt them into place, install the injector into the SIFT and proceed.

Given that all hole-pattern injectors work, it is still useful to address the issue of which is the best design. Inner inlet Type-D [Fig. 4(d)] is the one we consider the best for our SIFT apparatus; it has good ion efficiency (routinely achieves 2–10 kcps of $O^{\cdot+}$ after 150 cm of flow tube at 0.4–0.5 Torr of He) while keeping the source region pressure in a workable range. Inner inlets A and C are also good but they have a reduced "pumping efficiency" compared to D. These three inner inlets (A, C, D) all have the buffer gas inlet holes on a planar surface and have a small separation between the gas inlet "plane" and the plane containing the ion entrance orifice. In contrast, hole-pattern inlets wherein the holes are in a sloped surface show less favorable characteristics.

If we were to build an injector flange from scratch what would we recommend? Our best guess is as follows: (1) use hole-pattern inlets; (2) use a 2–3 mm ion injection orifice; (3) use 12 holes of 0.2 mm diameter each for a reaction region with a long "turbulence damping region" and 0.34 mm diameter for short one; (4) keep the buffer gas inlet holes in a planar surface (not on a sloped surface); (5) minimize the separation of the plane containing the ion entrance orifice and the buffer gas inlet holes; (6) do not bother with outer inlets; (7) use aluminum and drill bits for construction.

Acknowledgements

The authors acknowledge valuable assistance from the University of Pittsburgh Chemistry Department's Model Shop and especially thank Thomas M. Gasmire for technical support and fabrication of our inlets. We also gratefully acknowledge support from the National Science Foundation.

References

[1] N.G. Adams, D. Smith, Int. J. Mass Spectrom. Ion Phys. 21 (1976) 349.
[2] D. Smith, N.G. Adams, Adv. At. Mol. Phys. 24 (1988) 1.

[3] F. Howorka, F.C. Fehsenfeld, D.L. Albritton, J. Phys. 12 (1979) 4189.
[4] G.I. Mackay, G.D. Vlachos, D.K. Bome, H.I. Schiff, Int. J. Mass Spectrom. Ion Phys. 36 (1980) 259.
[5] G. Dupeyrat, B.R. Rowe, D.W. Fahey, D.L. Albritton, Int. J. Mass Spectrom. Ion Phys. 44 (1982) 1.
[6] T.M. Miller, R.E. Wetterskog, J.F. Paulson, J. Chem. Phys. 80 (1984) 4922.
[7] J.M. Van Doren, S.E. Barlow, C.H. DePuy, V.M. Bierbaum, Int. J. Mass Spectrom. Ion Processes 81 (1987) 85.
[8] J.M. Van Doren, Ph.D. Thesis, University of Colorado, Boulder, CO, 1987.
[9] T.S. Graul, R.R. Squires, Mass Spectrom. Rev. 7 (1988) 263.
[10] S. Kato, M.J. Frost, V.M. Bierbaum, S.R. Leone, Rev. Sci. Instrum. 64 (1993) 2808.
[11] P.J. Marinelli, J.A. Paulino, L.S. Sunderlin, P.G. Wenthold, J.C. Poutsma, R.R. Squires, Int. J. Mass Spectrom. Ion Processes 130 (1994) 89.
[12] M. Iraqi, A. Petrank, M. Peres, C. Lifshitz, Int. J. Mass Spectrom. Ion Processes 100 (1990) 679.
[13] G.K. King, M.M. Maricq, V.M. Bierbaum, C.H. DePuy, J. Am. Chem. Soc. 103 (1981) 7133.
[14] G.O. Brink, Rev. Sci. Instrum. 37 (1966) 857.
[15] M. McFarland, D.L. Albritton, F.C. Fehsenfeld, E.E. Ferguson, A.L. Schmeltekopf, J. Chem. Phys. 59 (1973) 6610.
[16] J.J. Grabowski, C.H. DePuy, V.M. Bierbaum, J. Am. Chem. Soc. 105 (1983) 2565.
[17] D.R. Miller, in Atomic and Molecular Beam Methods, G. Scoles (Ed.), Oxford University, New York, 1988, Vol. 1, Chap. 2.
[18] K. Bier, B. Schmidt, Z. Angew. Phys. 13 (1961) 493.
[19] W. Lindinger, D.L. Albritton, J. Chem. Phys. 62 (1975) 3517.